Received: 5 November 2021 | Revised: 29 March 2022 | Accepted: 10 April 2022

DOI: 10.1002/joc.7663

RESEARCH ARTICLE

International Journal of Climatology RMetS

Relationship between frontal systems and extreme precipitation over southern South America

Florencia I. Solari[1] | **Josefina Blázquez**[1] | **Silvina A. Solman**[2]

[1]Facultad de Ciencias Astronómicas y Geofísicas, Universidad Nacional de La Plata (FCAG/UNLP), Buenos Aires, Argentina

[2]Centro de Investigaciones del Mar y la Atmósfera (CIMA-CONICET/FCEN-UBA), Instituto Franco Argentino del Clima y sus Impactos (UMI IFAECI/CNRS), Departamento de Ciencias de la Atmósfera y los Océanos (FCEN-UBA), Ciudad Universitaria, Buenos Aires, Argentina

Correspondence
Florencia I. Solari, Facultad de Ciencias Astronómicas y Geofísicas, Universidad Nacional de La Plata (FCAG/UNLP), Paseo del Bosque s/n, B1900FWA, La Plata, Buenos Aires, Argentina.
Email: fsolari@fcaglp.unlp.edu.ar

Funding information
Consejo Interuniversitario Nacional, Grant/Award Number: EVC-CIN 2019; Fondo para la Investigación Científica y Tecnológica, Grant/Award Number: PICT2018-02496; Universidad de Buenos Aires, Grant/Award Number: UBACYT2018 20020170100117BA; UNLP, Grant/Award Number: PPID/G006

Abstract

The relationship between frontal systems and extreme precipitation events over southern South America is analysed for the austral winter (May–August) and spring (September–December), on a 39-year period spanning from 1979 to 2017. Daily gridded data from the CPC Global Unified Precipitation dataset and the ERA5 reanalysis are employed. Fronts are identified by means of an objective front index (FI) that takes into account both dynamic (cyclonic vorticity) and thermodynamic (thermal contrast) characteristics. Extreme precipitation is characterized by the seasonal 95th percentile. Fronts occur in mid-latitudes in about 10% of the days but there is a seasonal shift with larger occurrence frequencies located at southern latitudes in spring compared to winter. Front intensity—calculated as the seasonal mean of FI—is stronger in winter than in spring but the spatial pattern is similar on both seasons. Fronts explain about 50% of extreme precipitation on winter and 40% on spring; the percentage of total precipitation explained by fronts is lower but the spatial distribution is similar. Comparison between fronts that produce precipitation and the ones associated with extreme precipitation revealed that the latter are more intense on average. Fronts that produce extreme precipitation have a stronger dynamic forcing (i.e., higher cyclonic vorticity values) and a higher moisture availability (higher specific humidity anomaly). These two characteristics are the most promising for enhancing extreme precipitation events forecast.

KEYWORDS

ERA5, extreme precipitation, fronts, South America

1 | INTRODUCTION

South America has a considerable meridional extension, exhibiting diverse patterns of weather and climate (Garreaud *et al.*, 2009; Reboita *et al.*, 2010), and a complex topography of which the most prominent feature is the Andes Cordillera that runs along the west coast and has an altitude greater than 4 km in most parts. This continent experiences varied types of transient perturbations, of both tropical and extratropical origin, and on varied scales, from synoptic and mesoscale to organized and disorganized convection, with cold front passages being the most common transient weather events over the continent (Satyamurty *et al.*, 1998; Garreaud, 2000; Loikith *et al.*, 2019).

Extreme precipitation events have great socioeconomic impact; flooding caused by these events are often associated with casualties and material losses, while also impacting on various activities, such as farming, cattle raising, transportation, tourism, energy generation and

distribution (Carleton and Hsiang, 2016). Vörösmarty *et al.* (2013) evaluated the risk from extreme precipitation and floods in urban and rural areas of South America as combination of social and natural factors and determined that climate change and climate variability (specially in future decades) contribute in shaping and increasing the risk. In addition, the last IPCC report (Masson-Delmotte *et al.*, 2021) projects an increase in extreme precipitation over various regions of the world that leads to flooding becoming more frequent at the end of the century.

In the past few years, numerous studies based on observed data have found an increase in the trends of extreme precipitation over various regions of South America (Haylock *et al.*, 2006; Re and Barros, 2009; Penalba and Robledo, 2010; Wu and Polvani, 2017; Dereczynski *et al.*, 2020). Over south-eastern South America (SESA), Re and Barros (2009) found that heavy precipitation became more frequent and intense in the last decades (1959–2002); these trends could be explained by an increase of available moisture (due to positive trends in minimum temperature) and an increase of instability. Over the same region and in a similar period (1961–2000), Penalba and Robledo (2010) found that there is a positive annual trend in the number of daily extreme rainfall events—defined by the 75th percentile. Wu and Polvani (2017) found that the stratospheric ozone depletion induces changes on the low-level atmospheric circulation (low-level convergence, cyclonic circulation, enhanced ascent) over SESA that lead to increased precipitation, favouring the occurrence of heavier rainfall extremes. Haylock *et al.* (2006) evaluated the precipitation trends (1960–2000) through various indexes, like the number of heavy precipitation days or the amount of extreme precipitation accumulated on a year, and found large regions of coherent change, with a shift to wetter conditions in central and northern Argentina, Paraguay, and southern Brazil, and negative trends in southern Chile and southwestern Argentina. Dereczynski *et al.* (2020) analysed the precipitation trends for the 1969–2000 period trough annual indexes representing total and extreme precipitation and found a tendency towards wetter conditions over most of South America, however, less than 10% of the series had statistical significance.

Synoptic-scale fronts are one of the most important meteorological systems producing precipitation, more so in mid-latitudes (between 30° and 60° parallels, in both hemispheres). These systems are associated with ascending air, clouds, and precipitation—depending on moisture availability, stability conditions and other factors—(Bjerknes and Solberg, 1922; Browning and Roberts, 1994; Lackmann, 2011). Simmonds *et al.* (2012) and Schemm *et al.* (2015) studied the frontal activity using various metrics and found that the highest frequencies in the Southern Hemisphere occur between 40°S and 60°S. In South America, Satyamurty *et al.* (1998) observed (between 5°S and 40°S) that there are frontal occurrences all year round, but their frequency diminishes towards lower latitudes.

Traditionally, fronts are identified by means of manual (subjective) analysis of various meteorological charts, but they can also be identified using automated (objective) methods (Escobar *et al.*, 2019). The automated identification of fronts by using fundamental variables which are well handled by the models facilitates the production of frontal climatologies (Hewson, 1998). The most commonly used automated methods employ horizontal gradients of thermodynamical variables that may contain moisture—like the equivalent potential temperature and the wet-bulb potential temperature—(Hewson, 1998; Berry *et al.*, 2011; Catto *et al.*, 2012; Catto and Pfahl, 2013; Catto *et al.*, 2014; Hope *et al.*, 2014; Schemm *et al.*, 2015; Dowdy and Catto, 2017), usually calculated at the 850 hPa isobaric level although, recently, dynamical criteria—based on the temporal shifts of the horizontal wind (usually, in the 10 m level or the 850 hPa level)—are being used in automated front identification (Simmonds *et al.*, 2012; Hope *et al.*, 2014; Schemm *et al.*, 2015; Rudeva *et al.*, 2019). There are other methods based on both dynamical and thermodynamical characteristics (like vorticity and temperature gradient, respectively) used to identify fronts (Solman and Orlanski, 2010; Solman and Orlanski, 2014; Blázquez and Solman, 2016; Blázquez and Solman, 2017; Parfitt *et al.*, 2017) that can also include moisture availability (Blázquez and Solman, 2018; Blázquez and Solman, 2019). Some authors (Berry *et al.*, 2011; Hope *et al.*, 2014; Schemm *et al.*, 2015) also added a minimum length condition to the features identified by the criteria mentioned above, like three adjacent grid points or an extent of at least 500 or 1,000 km.

Schemm *et al.* (2015) found that, especially in the Southern Hemisphere, fronts can be positioned in different places depending on which criterion is used, so cold fronts identified by wind changes (dynamical criterion) were located poleward of those identified by the equivalent potential temperature (thermodynamical criterion); these differences can be partially explained by the position of the storm tracks—located at higher latitudes in the Southern Hemisphere where the atmosphere is drier and the moisture gradients are weaker—and due to the fact that thermodynamical-based methods (like those shown by Hewson, 1998) are better suited to the Northern Hemisphere's synoptic characteristics. Berry *et al.* (2011) observed that there are real boundaries in the wet-bulb potential temperature (used to identify

fronts) that are not meteorological fronts; instead, they are caused by persistent baroclinic zones connected with a change in the underlying surface or sloping terrain. These authors did not define a way to avoid detecting these zones or classifying them as—quasi-stationary—fronts.

In recent years, numerous studies have examined the relationship between precipitation and fronts. Catto *et al.* (2012) found that up to 90% of precipitation in the storm tracks regions comes from fronts and that there is a regional and seasonal variation of the proportion of precipitation associated with fronts. Blázquez and Solman (2018), who also studied this relationship, found that in extratropical latitudes around 40% of the precipitation occurs in the presence of a front, whereas in some regions—such as SESA and between 60°S and 70°S—more than 60% of the precipitation is caused by frontal systems. Solman and Orlanski (2014) documented the poleward shift in frontal activity during the last decades and the close correspondence between precipitation and frontal activity both in the spatial pattern of the changes and the temporal evolution of anomalies at high and mid-latitudes of the South Hemisphere, suggesting that precipitation changes are strongly controlled by changes in frontal activity. Recently, Blázquez and Solman (2016) and Blázquez and Solman (2017) analysed the variability of the frontal activity and its relationship with large-scale atmospheric circulation and precipitation variability in both intraseasonal and interannual scales. Blázquez and Solman (2016) suggested that the intraseasonal variability of fronts is controlled by the large-scale atmospheric circulation and that, in turn, the intraseasonal variability of fronts modulates the precipitation anomalies on the same timescale. Blázquez and Solman (2017) found that both the SAM and the ENSO-mode influence the leading mode of the fronts variability, which in turn controls the interannual variability of precipitation over southern South America and adjacent oceans.

While the relationship between frontal systems and precipitation has been extensively studied on the Southern Hemisphere, the correspondence between fronts and extreme precipitation has yet to be explored in depth. Cavalcanti (2012) studied various cases of floodings and precipitation extremes in South America in the early 21st century and found that extreme precipitation occurs mostly within mesoscale convective complexes embedded within synoptic-scale systems such as frontal zones. Hirata and Grimm (2016) and Hirata and Grimm (2017) studied the role of synoptic and intraseasonal anomalies during extreme rainfall events and found that these events are mainly driven by synoptic disturbances propagating equatorward east of the Andes associated with intense fronts and cold air incursions. On a global scale, Catto and Pfahl (2013) found that in the midlatitudes, fronts are responsible for up to 90% of the extreme precipitation events, rendering fronts as the most relevant forcing. This relationship has not been analysed in depth on a regional scale over a continent with complex topography like South America.

The aim of this study is to analyse the relationship between frontal systems and extreme precipitation over southern South America. The specific goals are (a) to characterize both the frontal activity and the extreme precipitation over southern South America for different seasons; (b) to explore the proportion of extreme precipitation explained by fronts on different seasons; (c) to analyse distinctive characteristics of fronts that produce extreme precipitation. This paper is divided into four sections: section 2 describes the data and methods employed; results are discussed on section 3; on section 4, a brief summary is presented along with the conclusions of this work.

2 | DATA AND METHODS

2.1 | Data

The study region spans from 33°W to 83°W and from 15°S to 60°S, encompassing southern South America, although the focus of the analysis is on the mid-latitudes. The time period considered starts in 1979 and ends in 2017 (39 years) and it is divided into two seasons of interest: extended winter or MJJA (May, June, July, August) and extended spring or SOND (September, October, November, December). According to Blázquez and Solman (2018), the austral extended winter is the period when the strongest relationship between fronts and precipitation is expected to occur in the Southern Hemisphere. In the extended spring, a relative decline of the relative importance of fronts is expected since other precipitation forcing become more frequent (like thermal forcing), but an increase in the accumulated precipitation is also expected.

Two gridded data sets with daily values are used. Daily accumulated precipitation data are taken from the CPC Global Unified Precipitation dataset provided by the NOAA/OAR/ESRL (Xie *et al.*, 2010) and have a horizontal resolution of $0.5° \times 0.5°$ only over continental landmasses. Data from the newly developed ERA5 (Urraca *et al.*, 2018; Hersbach *et al.*, 2020) from the European Centre for Medium-Range Weather Forecast (ECMWF) is also used. Its horizontal resolution is $0.25° \times 0.25°$ and, although the native temporal resolution is hourly, a daily mean is taken so the data used has daily values. The variables employed are the 850 hPa temperature, zonal and

meridional wind components, and specific humidity; terrain elevation is extracted from the same database. The number of grid points of ERA5 is four times higher than that of the CPC database; however, all grid points of the precipitation data match a grid point of the ERA5 data. Since the analysis performed is not done on a "point by point" basis (instead, it is based on a nearness approach), this partial matching of the grids is enough to avoid interpolating one data set (and thus, either losing data or introducing an error source) and each one can be used in its native horizontal resolution.

2.2 | Methods

2.2.1 | Extreme precipitation

Extreme precipitation is defined in each grid point, and for each season, using the 95th percentile of the precipitation series, using only the days in which the daily total is greater or equal than 1 mm. This means that the length of each precipitation series is not necessarily the same; therefore, the number of days with extreme precipitation (i.e., the days in which the daily total is greater than the threshold given by the 95th percentile) may differ in different grid points. The advantage of using a statistical definition that only takes into account the days with precipitation is that the extreme values obtained are referenced to the total precipitation and not to the total amount of days in the season; this exclusion of zeros and trace values (less than 1 mm·day^{-1}) that yields precipitation series of different lengths differs from others studies, such as Catto and Pfahl (2013), that use same-length series but obtain lower extreme thresholds.

2.2.2 | Frontal index

Fronts are identified and characterized by means of an objective index based on two fundamental characteristics of these mid-latitudes systems: cyclonic vorticity and thermal contrast. This front index (FI) was developed by Solman and Orlanski (2010) and it is computed at the 850 hPa isobaric level using

$$\mathrm{FI} = -\zeta \times |\nabla T| > 0, \quad (1)$$

where the factors on the right-hand side of Equation (1) are the relative vorticity ζ and the temperature gradient module $|\nabla T|$. Since only cyclonic vorticity is considered and it has negative values on the Southern Hemisphere, a -1 factor is included in Equation (1) so that FI results positive.

All grid points where the terrain elevation is greater than 800 m are masked prior to any computation. This condition is more strict than that typically used for the 850 hPa level, but its purpose is to filter the terrain influence on the atmosphere when this isobaric level is close to the surface. It drastically improves the characterization of fronts, eliminating a good number of false positives related to semipermanent intense thermal contrasts associated with sloping terrain (not shown).

In order to compute each factor of Equation (1), the daily zonal anomalies of the zonal and meridional components of the wind and the temperature are taken to highlight the wave patterns of weather systems. Then, the relative vorticity and the module of the temperature gradient are calculated using centred finite differences in spherical coordinates. Following Blázquez and Solman (2018), a minimum threshold for the temperature gradient ($|\nabla T| \geqslant 1\,^{\circ}\mathrm{C}/_{100\mathrm{km}}$) is used, eliminating weak thermal contrasts that are not front-related. A threshold is also used in the vorticity values ($|\zeta| \geqslant 5\times10^{-6}\mathrm{s}^{-1}$) in order to avoid weak cyclonic vorticity features.

Lastly, a nonpersistent condition is applied to keep transient perturbations and filter semi-permanent features that are not front-related. In this case, persistence is defined by the occurrence of more than three consecutive days marked as front (i.e., FI > 0) on a single grid point. Persistent events are not classified as fronts and are therefore excluded from the analysis. This filtering condition improves results on the edge of elevated terrain masked regions but does not particularly affect other regions (not shown).

After removing the persistent events, all grid points where FI > 0 are labelled as fronts. Consecutive—but not persistent—days with FI > 0 on the same grid point are considered as separate fronts. Front occurrence frequency is calculated, on each grid point, as the number of days with FI > 0 over the total number of days of the season on the whole period considered (4,797 days in winter—MJJA—and 4,758 days in spring—SOND).

Similar versions of this index have been used in various studies (Solman and Orlanski, 2010; Solman and Orlanski, 2014; Blázquez and Solman, 2016; Blázquez and Solman, 2017; Parfitt *et al.*, 2017; Blázquez and Solman, 2018; Blázquez and Solman, 2019) in the last decade and it has provided good results in the identification of frontal systems on an hemispheric basis.

2.2.3 | Linking fronts with precipitation

Precipitation is classified as front-related if there is a front nearby on the same day. Instead of searching for a front in a fixed number of grid points surrounding the

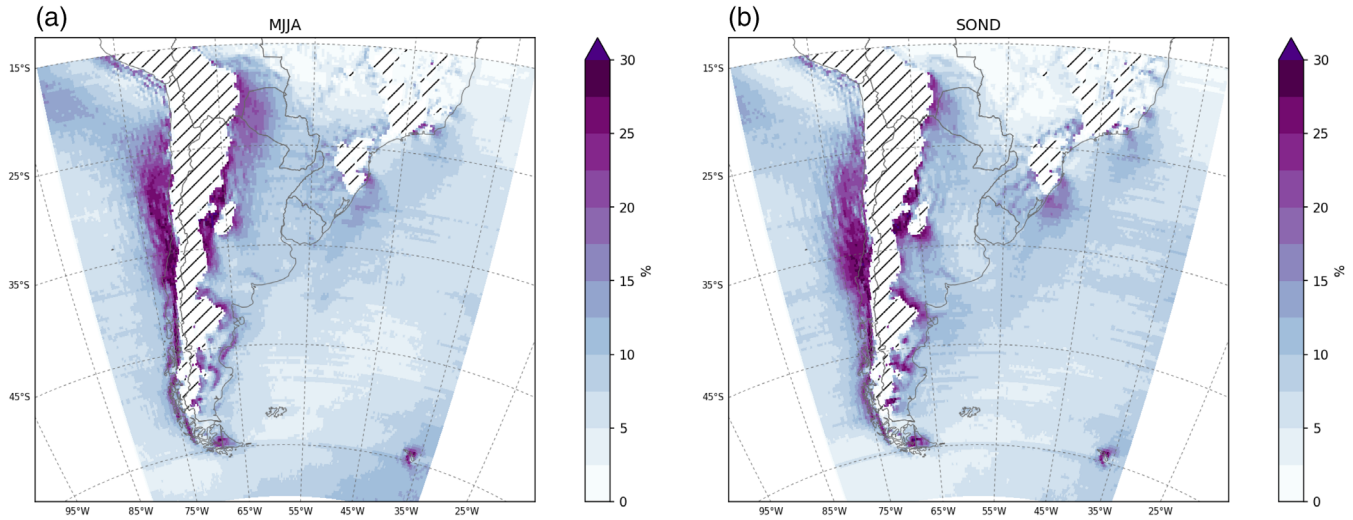

FIGURE 1 Front frequency (%) for (a) MJJA, (b) SOND. High terrain (over 800 m) is hatched [Colour figure can be viewed at wileyonlinelibrary.com]

precipitation event, a more organic approach is employed, taking into account a search area delimited by a fixed physical distance. The physical distance is the shortest distance that can be measured between any two points on a sphere following a path over the sphere's surface. This way of defining the delimiting distance ensures that the search area is the same for all latitudes (which does not happen when using a fixed number of grid points).

In this case, the maximum search distance from the precipitation event is set at 120 km, measured as the distance following a spherical surface by the haversine formula (Sinnott, 1984). Additionally, a minimum number of points marked as front (FI > 0) must exist within the search area in order to consider that the precipitation is in fact caused by a frontal system. This is not a fixed number, but a percentage of the points within the search area, so it is comparable in different latitudes. The minimum number of points that must have FI > 0 in order to classify the precipitation (central point) as frontal is 20% of the points encompassed within the search area delimited by the 120 km distance from the centre.

Some sensitivity tests (not shown) were done using different combinations of the maximum distance (from 100 to 200 km, with the latter being the most similar to the one used in literature) and minimum grid points percentage (ranging from 10% to 40%) and it was found that, while this method is not particularly sensitive to distance changes (within the same percentage value, excepting the smallest one), it becomes stricter with higher percentage values, resulting in less precipitation classified as frontal.

This new approach in spatial linking of precipitation and fronts is fairly robust and it represents an advantage compared with previous studies (Catto *et al.*, 2012; Catto and Pfahl, 2013; Dowdy and Catto, 2017; Blázquez and Solman, 2018; Blázquez and Solman, 2019) in that it handles different latitudes equally, and it is possible due to the high horizontal resolution of the ERA5 dataset.

3 | RESULTS

3.1 | Extreme precipitation and fronts

Frontal systems are described, in a climatological sense, by their frequency of occurrence and the mean value of the frontal index FI. Figure 1 shows the frequency of fronts for the austral extended winter (MJJA) and extended spring (SOND). Over the continent, fronts are present in about 10% of the days; these values are in concordance with previous studies (Berry *et al.*, 2011; Catto *et al.*, 2014; Blázquez and Solman, 2018), although the data and the automated detection methods used are different. There is a seasonal shift between winter (Figure 1a) and spring (Figure 1b); for the latter, the northern extent of fronts is shorter and frequency increases (decreases) in southern (central and northern) Argentina. Solman and Orlanski (2014) also documented the broader meridional extent of fronts in winter, consistent with the seasonal migration of the Southern Hemisphere storm track. Further comparison with other studies—that use thermodynamical variables (Berry *et al.*, 2011; Catto *et al.*, 2014) or a modified version of FI that includes humidity (Blázquez and Solman, 2018) to detect fronts—reveals that they found a relative maxima over southeastern Brazil (50°W, 28°S) whereas in the

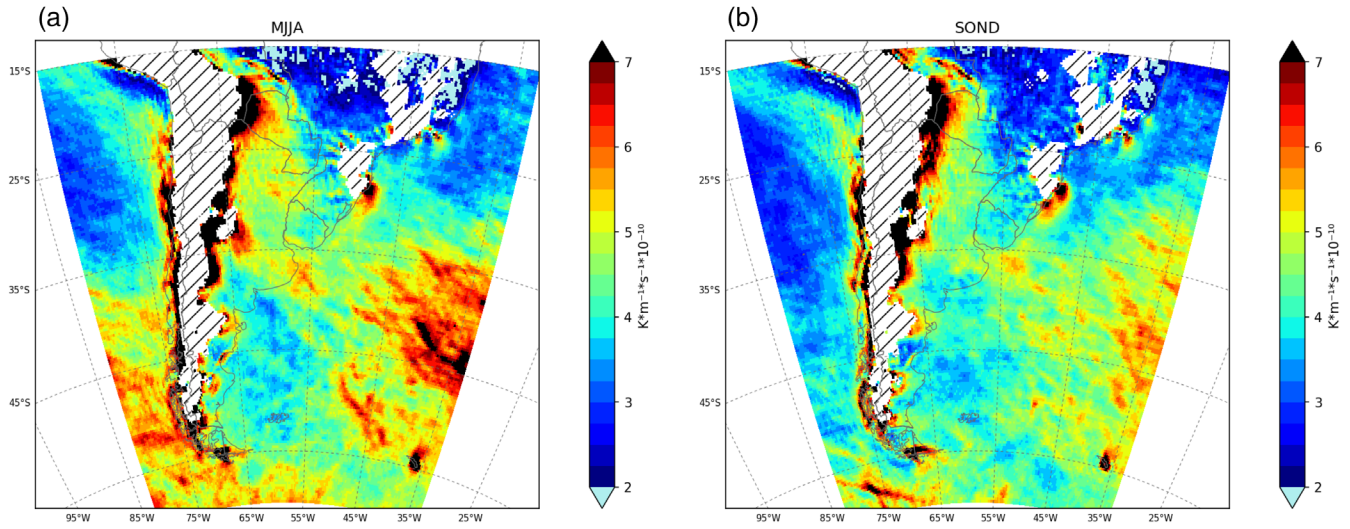

FIGURE 2 Front index (FI) seasonal mean for (a) MJJA, (b) SOND. Units are $K \cdot m^{-1} \cdot s^{-1} \times 10^{-10}$ [Colour figure can be viewed at wileyonlinelibrary.com]

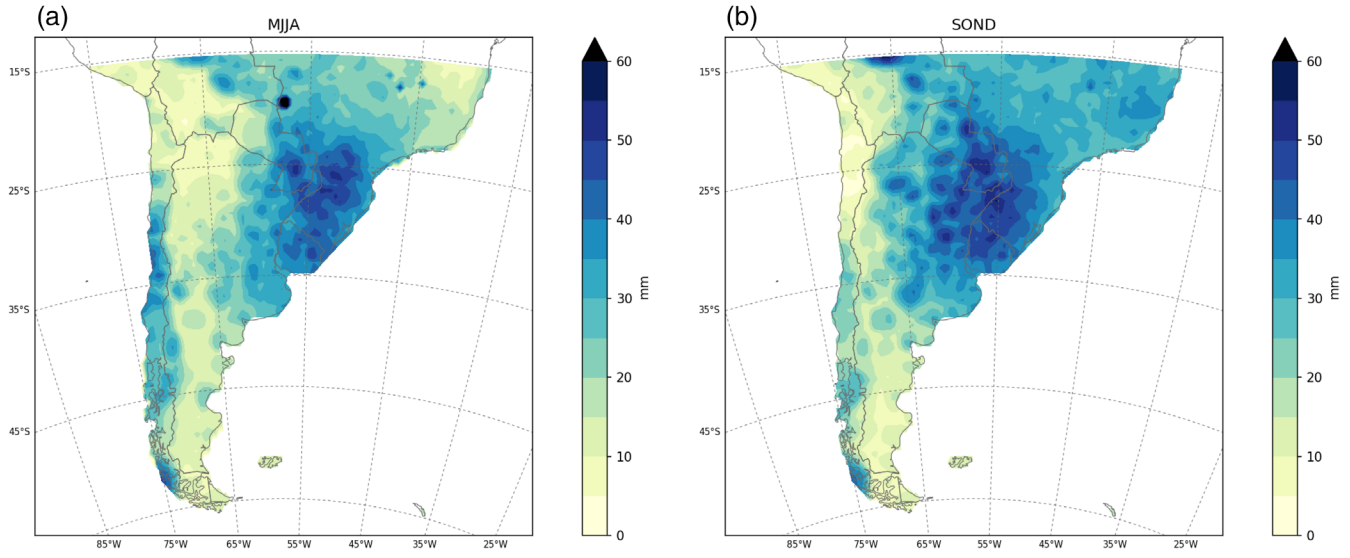

FIGURE 3 Precipitation 95th percentile—only taking into account days with daily accumulated greater or equal to 1 mm—for (a) MJJA, (b) SOND. Units are millimetres (mm) [Colour figure can be viewed at wileyonlinelibrary.com]

present case (Figure 1) the frequency cannot be calculated in this region due to high terrain masking.

The seasonal mean of FI is depicted in Figure 2 for both winter and spring. Only grid points classified as fronts (i.e., nonpersistent FI > 0) were used in these calculations. The spatial pattern of the mean FI is similar on both seasons but the values are higher in winter (Figure 2a) than in spring (Figure 2b). There are two minimums, one over the eastern Pacific Ocean (between 20°S and 40°S) likely associated to the semipermanent high-pressure system, and one over the Argentinean Sea (east of the Patagonia). Very high values are found in coastal areas and flanking the Andes due to intense vorticity and thermal contrast, while the lowest values are located north of 20°S where fronts are scarce. The spatial pattern in winter (Figure 2a) is quite similar to the one found by Blázquez and Solman (2018), although FI values cannot be compared because they used a modified version of the index. In addition, Solman and Orlanski (2014) also found FI seasonal mean values to be higher in winter; however, the index values are considerably larger in this study, likely due to the much higher spatial resolution of the data employed.

Extreme precipitation is characterized by the threshold given by the 95th percentile (Figure 3) and the number of days surpassing this threshold (Figure 4). The

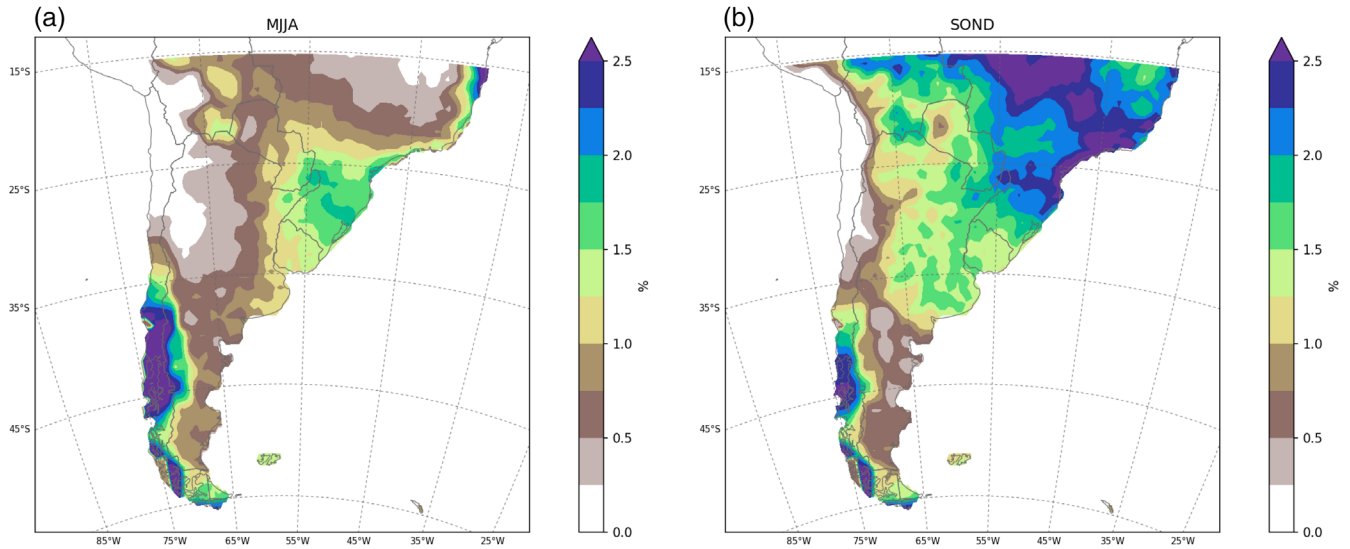

FIGURE 4 Number of days with extreme precipitation as a fraction of the total amount of days of the season for (a) MJJA—4,797 days total, (b) SOND—4,758 days total. Units are percentage [Colour figure can be viewed at wileyonlinelibrary.com]

highest values of the 95th percentile are located in southeastern South America (SESA) in both seasons, with larger values in spring. In Patagonia and central Andes the low values mark the South American arid diagonal (Bruniard, 1982; Garreaud *et al.*, 2009), whereas the Chilean coast showcases higher values south of 30°S, particularly in winter. In northwestern Argentina and north of 20°S in Brazil there is a marked seasonal shift, with low values in winter and higher values in spring. Figure 3a is in agreement (in spatial distribution as well as numerical values) with the winter climatology of Reboita *et al.* (2022), even though the analysed periods differ and they use a 3-month season instead of the extended 4-month one employed here. The spatial pattern of the 95th percentile of precipitation matches the one found by Hirata and Grimm (2017) but the values on the present study are higher due to the exclusion of non-precipitation days (daily accumulated less than 1 mm), which yields higher threshold values, thus allowing a better characterization of precipitation extremes.

The number of days with extreme precipitation depends on the number of precipitation days, and while the former represents 5% of the latter (given that it is defined by means of the 95th percentile), both quantities vary within the domain. The number of days with extreme precipitation (Figure 4) is less than 2.5% of the total number of days in each season for the study period (4,797 days in MJJA and 4,758 days in SOND). On both seasons, regions with a higher (lower) number of days with extreme precipitation also have higher (lower) 95th percentile values. On the southernmost part of the continent—excepting the western coast—there are few days with extreme precipitation (less than 1%). In winter, there is a relative maximum in SESA (around 1.5%) while the surrounding regions have very low values. In spring, the highest values are located in tropical Brazil (around 2.5%) but there are also high values in northeastern Argentina (around 1.5%).

Each precipitation event is classified as either frontal or nonfrontal, depending on whether there is a front nearby or not (conditions are described in section 2.2.3). The ratio between the precipitation associated with fronts (taken as the sum of all frontal daily totals) and the total precipitation accumulated in the season for the whole period yields the percentage of precipitation linked to fronts (Figure 5a,b). On both seasons, frontal precipitation is mostly confined south of 20°S, given that fronts are mid-latitudes systems. In winter (Figure 5a), 40% of the total precipitation can be attributed to fronts, whereas in spring (Figure 5b) this percentage is lower—except in the southern part of the continent. This diminution can be explained by the increased importance—in warmer seasons—of other precipitation forcing mechanisms (like thermal forcing or precipitation produced by mesoscale convective systems). Also in spring, there are very low values in the northern part of the region with frontal precipitation, caused by the seasonal shift of weather systems.

The same approach is used with extreme precipitation events, taking the ratio between the extreme precipitation associated with fronts and the total extreme precipitation. The spatial distribution of extreme precipitation linked to fronts (Figure 5c,d) is similar to that of precipitation associated with frontal systems (Figure 5a,b), but the percentage explained is larger for the former. In winter (Figure 5c), around 50% of extreme precipitation can be

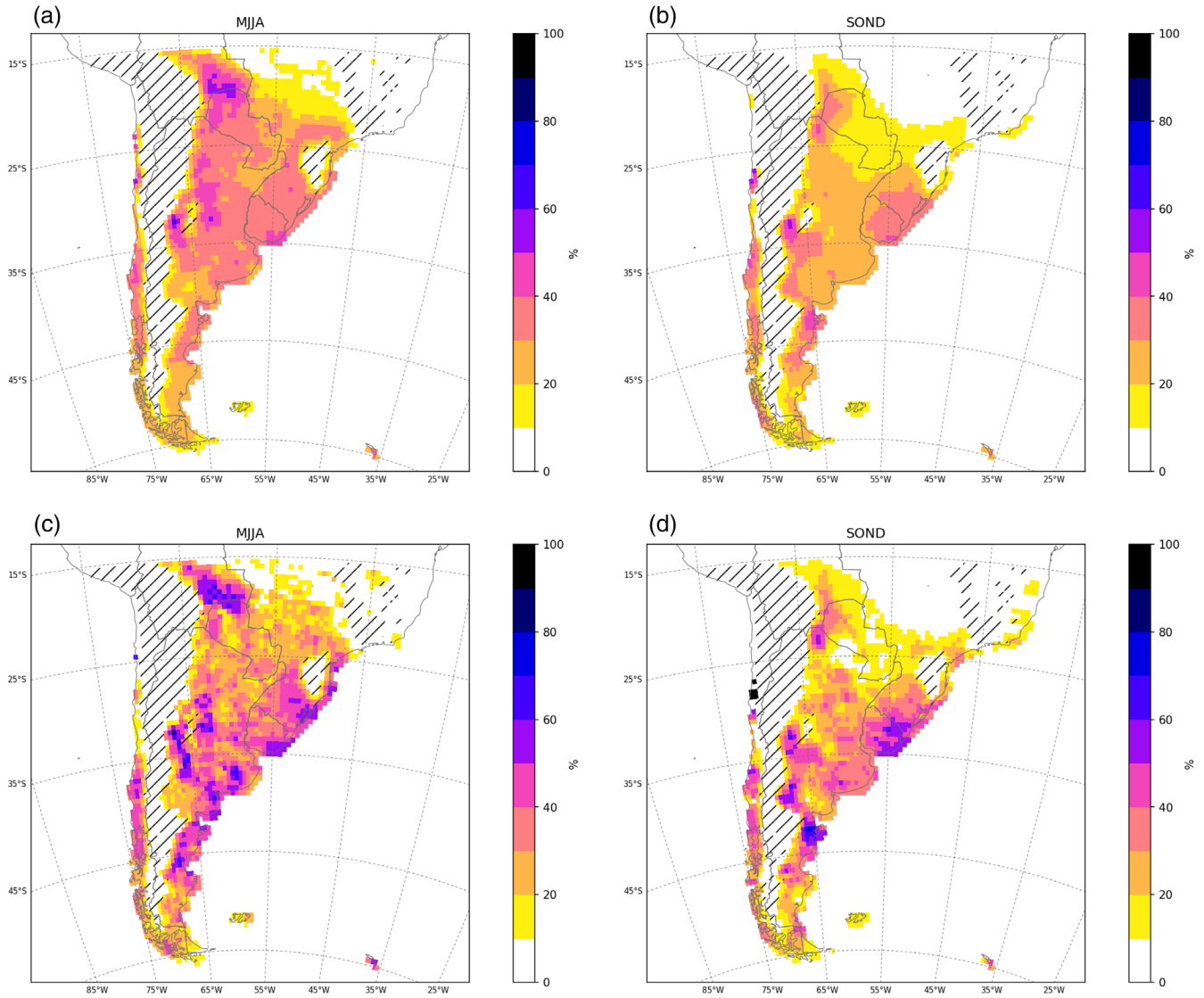

FIGURE 5 Top row: percentage of precipitation associated with fronts for (a) MJJA, (b) SOND. Bottom row: percentage of extreme precipitation associated with fronts for (c) MJJA, (d) SOND [Colour figure can be viewed at wileyonlinelibrary.com]

attributed to fronts, whereas in spring (Figure 5d) the percentage is about 40%. Accordingly, frontal systems seem to be an important forcing mechanism in triggering extreme precipitation events in southern South America.

Comparisons with previous studies should be cautiously handled since the approach used in each work can influence the results. For example, differences may arise from the data employed and its resolution, the method used in detecting fronts, the definition of extreme precipitation (see section 2.2.1), and the size and shape of the search area used for linking precipitation and fronts (see section 2.2.3). In general, the percentage of precipitation associated with fronts found in previous studies (Catto *et al.*, 2012; Catto and Pfahl, 2013; Blázquez and Solman, 2018) is higher than the values found here, but the linking criteria employed in this work is stricter. Blázquez and Solman (2018) found that in the extended austral winter at mid-latitudes the percentage of precipitation associated with fronts ranges from 40% to 60% but over SESA more than 60% of the total precipitation is due to frontal systems; these values are about 20% higher than those depicted in Figure 5a. Catto *et al.* (2012) found that, at mid-latitudes, up to 68% of the annual precipitation is associated with a front while this percentage is about 90% over SESA and 60% over Patagonia. However, they noted that these values are very sensitive to the size of the search area employed. Catto and Pfahl (2013) found similar results to this last study, with values over southern South America about 10% lower when using a stricter temporal condition.

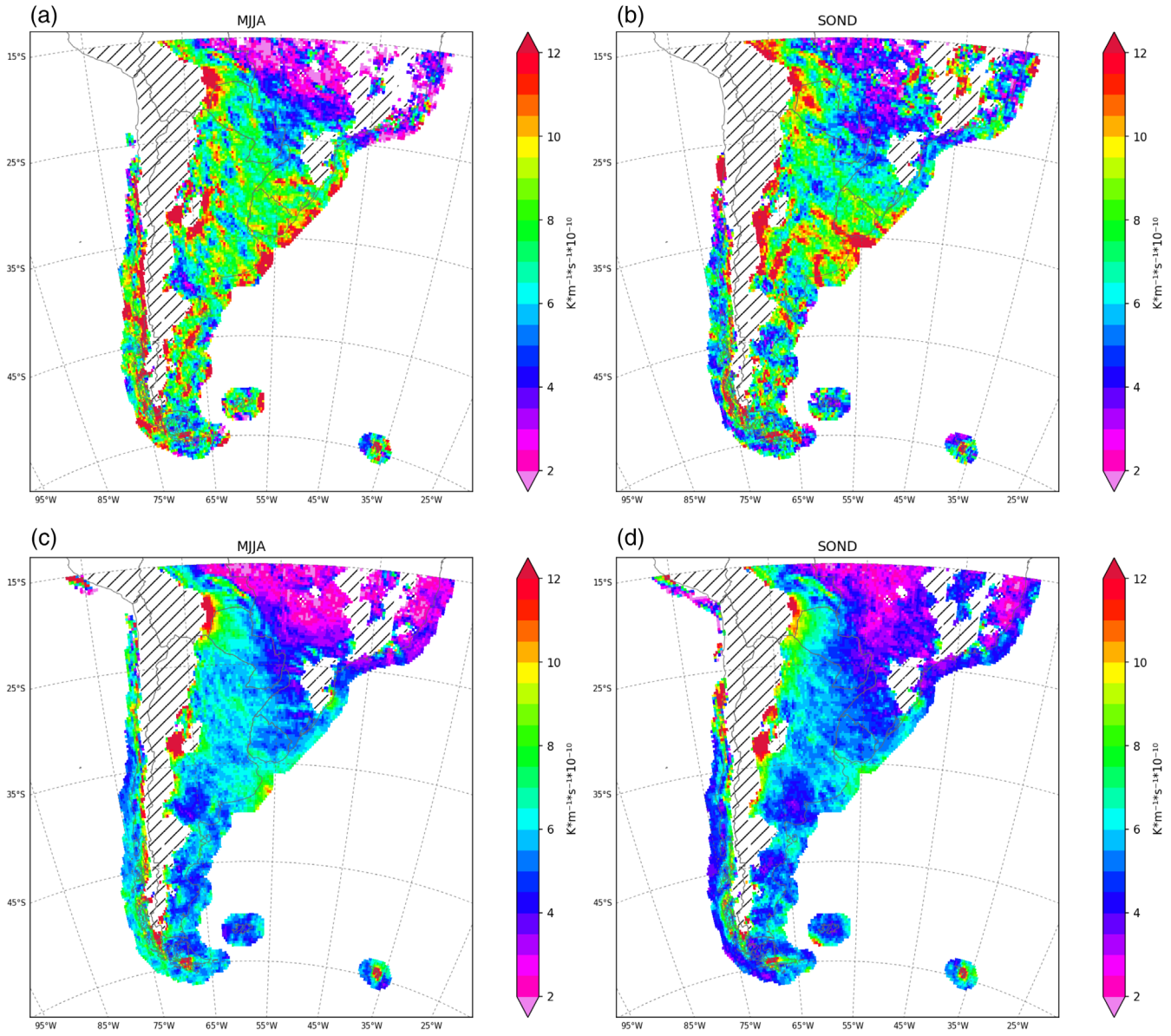

FIGURE 6 Top row: mean of FI for fronts that produce extreme precipitation for (a) MJJA, (b) SOND. Bottom row: mean of FI for fronts that produce precipitation for (c) MJJA, (d) SOND. Units are $K \cdot m^{-1} s^{\cdot -1} \times 10^{-10}$ [Colour figure can be viewed at wileyonlinelibrary.com]

3.2 | Characteristics of frontal systems associated with extreme precipitation

Frontal systems that trigger extreme precipitation may have distinctive characteristics that could be used in extreme events forecasting. Therefore, a comparison between various parameters associated with these fronts and with precipitating fronts (i.e., fronts that produce precipitation) is performed.

Grid points belonging to precipitating fronts are identified using a similar approach to the one described in section 2.2.3 to classify precipitation as either frontal or nonfrontal. That is, whenever the number of front points (FI > 0) surrounding the precipitation central point are enough to label the precipitation as front-related, these same points are classified as belonging to a precipitating front. In a similar fashion, grid points belonging to extreme-precipitation-producing fronts can also be identified. Thus, by identifying which points belong to either precipitating fronts or extreme-precipitation-producing fronts, two data subsets can be created. On each subset, and matching the grid points previously identified, composites of different variables are computed.

It should be noted that this approach cannot evaluate causality; however, it is fair to assume that whenever precipitation and a front simultaneously occur over the same region (as per the conditions described above and in section 2.2.3), the corresponding front is probably the

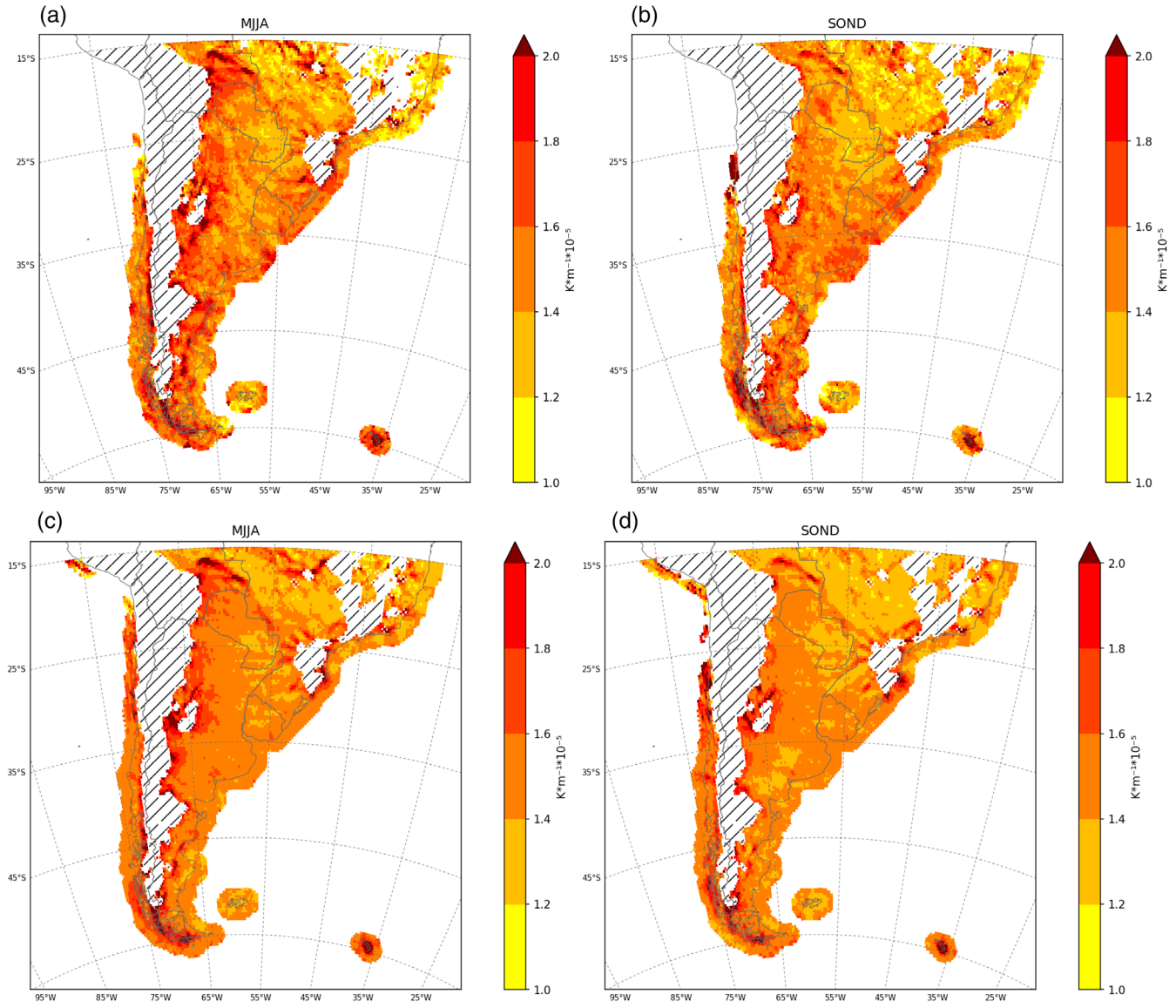

FIGURE 7 Top row: mean magnitude of the temperature gradient ($\nabla T \geq 1^{\circ}\mathrm{C}/_{100\mathrm{km}}$) for fronts that produce extreme precipitation for (a) MJJA, (b) SOND. Bottom row: mean magnitude of the temperature gradient ($\nabla T \geq 1^{\circ}\mathrm{C}/_{100\mathrm{km}}$) for fronts that produce precipitation for (c) MJJA, (d) SOND. Units are $K \cdot m^{-1} \times 10^{-5}$ [Colour figure can be viewed at wileyonlinelibrary.com]

dynamical forcing that ultimately triggers the precipitation event. In this sense, the front is considered as the precipitation triggering mechanism and it is consequently labelled as a precipitating front. Similar assumptions have been made, albeit sometimes implicitly, on previous studies (Catto and Pfahl, 2013; Dowdy and Catto, 2017; Blázquez and Solman, 2018; Blázquez and Solman, 2019).

To begin with, as a measure of front intensity, the mean value of the FI index (Figure 6) is compared for each type of precipitation-producing front and for both seasons. There are essentially no seasonal differences between mean FI values of fronts associated with extreme precipitation (Figure 6a,b), whose values are near 8×10^{-10} K·m^{-1}·s^{-1} despite some localized variations. However, these fronts are—on average—more intense than both precipitating fronts (Figure 6c,d) and all fronts (Figure 2a,b). Precipitating fronts do exhibit seasonal changes, with higher FI mean values in winter (Figure 6c) than in spring (Figure 6d); mean FI values in winter are near 6×10^{-10} K·m^{-1}·s^{-1} while in spring they are around 4×10^{-10} K·m^{-1}·s^{-1}. The mean intensity of precipitating fronts is also more spatially homogeneous than that of extreme-precipitation-producing fronts. This has to do with the fact that extreme precipitation is a very discontinuous variable—even more than precipitation—both spatially and temporally and the sample size is considerably smaller than that of the total precipitation sample.

Since any of the factors of FI (see Equation (1)) could contribute to the aforementioned observed differences in

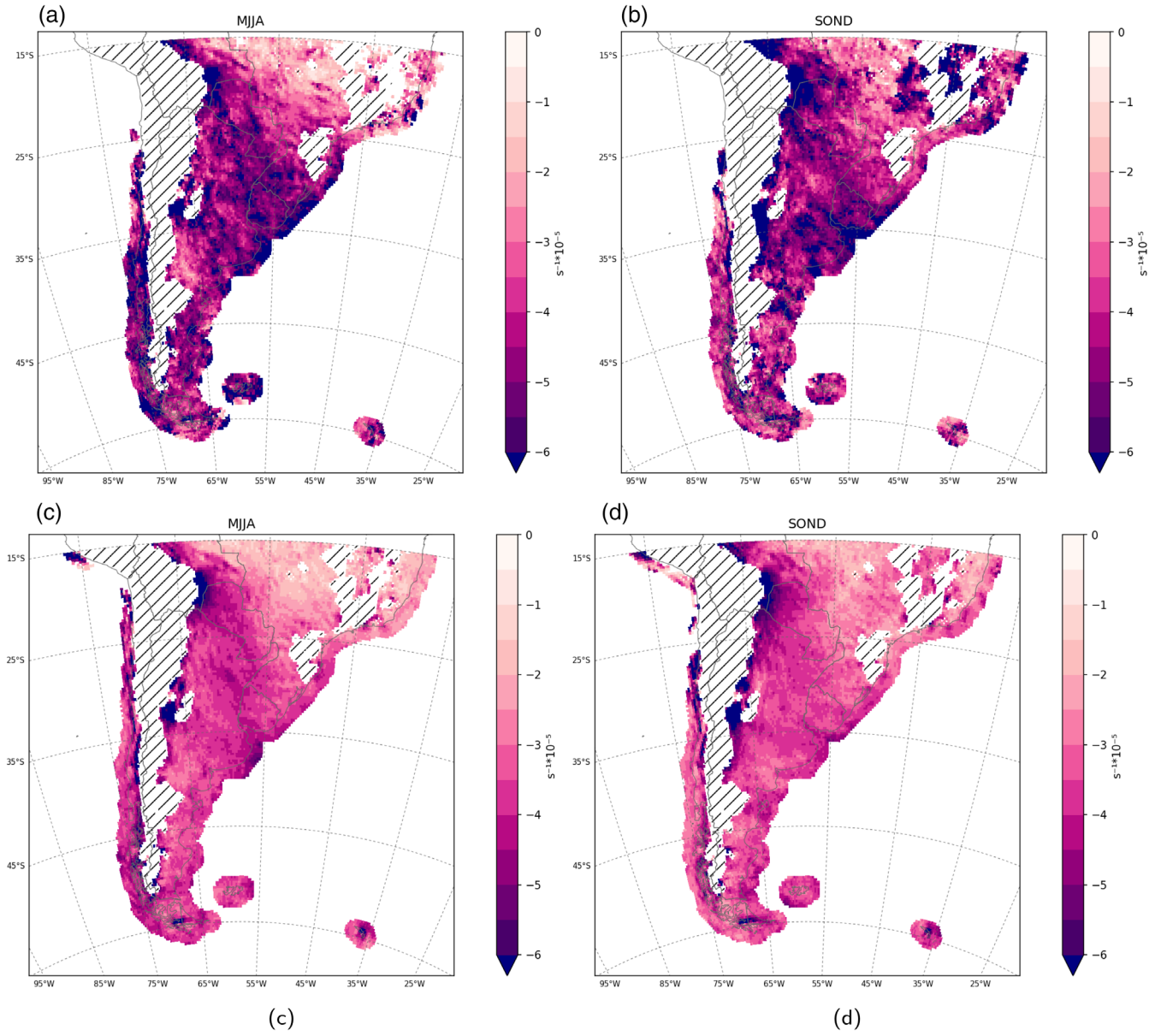

FIGURE 8 Top row: mean cyclonic vorticity (ζ<0) for fronts that produce extreme precipitation for (a) MJJA, (b) SOND. Bottom row: mean cyclonic vorticity (ζ<0) for fronts that produce precipitation for (c) MJJA, (d) SOND. Units are $s^{-1} \times 10^{-5}$ [Colour figure can be viewed at wileyonlinelibrary.com]

the mean of FI, the mean of each factor (cyclonic vorticity and magnitude of the temperature gradient) is calculated for both precipitating fronts and extreme-precipitation producing fronts in each season. In mid-latitudes, the mean magnitude of the temperature gradient is about 1.5×10^{-5} K·m^{-1} for both types of precipitation-producing fronts and for both winter and spring (Figure 7). On the other hand, the mean (cyclonic) vorticity of extreme-precipitation-producing fronts has values around -5.5×10^{-5} s^{-1} for both winter (Figure 8a) and spring (Figure 8b), thus being more intense than the mean for precipitating fronts (Figure 8c,d), which values are near -3.5×10^{-5} s^{-1}; however, there are basically no seasonal differences within each front type. In consequence, the observed differences in the mean of FI are mostly explained by the vorticity factor and not by thermal contrasts, which means that the dynamic aspect prevails over the thermodynamic aspect.

According to Bluestein (1993), the greater the thermal contrast, the smaller the frontal slope, and the greater the absolute vorticity magnitude, the greater the slope. This suggests that fronts that produce extreme precipitation could have, on average, greater slopes than precipitating fronts; however, this implication is not further explored since it does not pertain to the objectives of this study.

Fronts represent the triggering mechanism forcing air to move upward and, eventually, inducing condensation, cloud development and precipitation. However, moisture

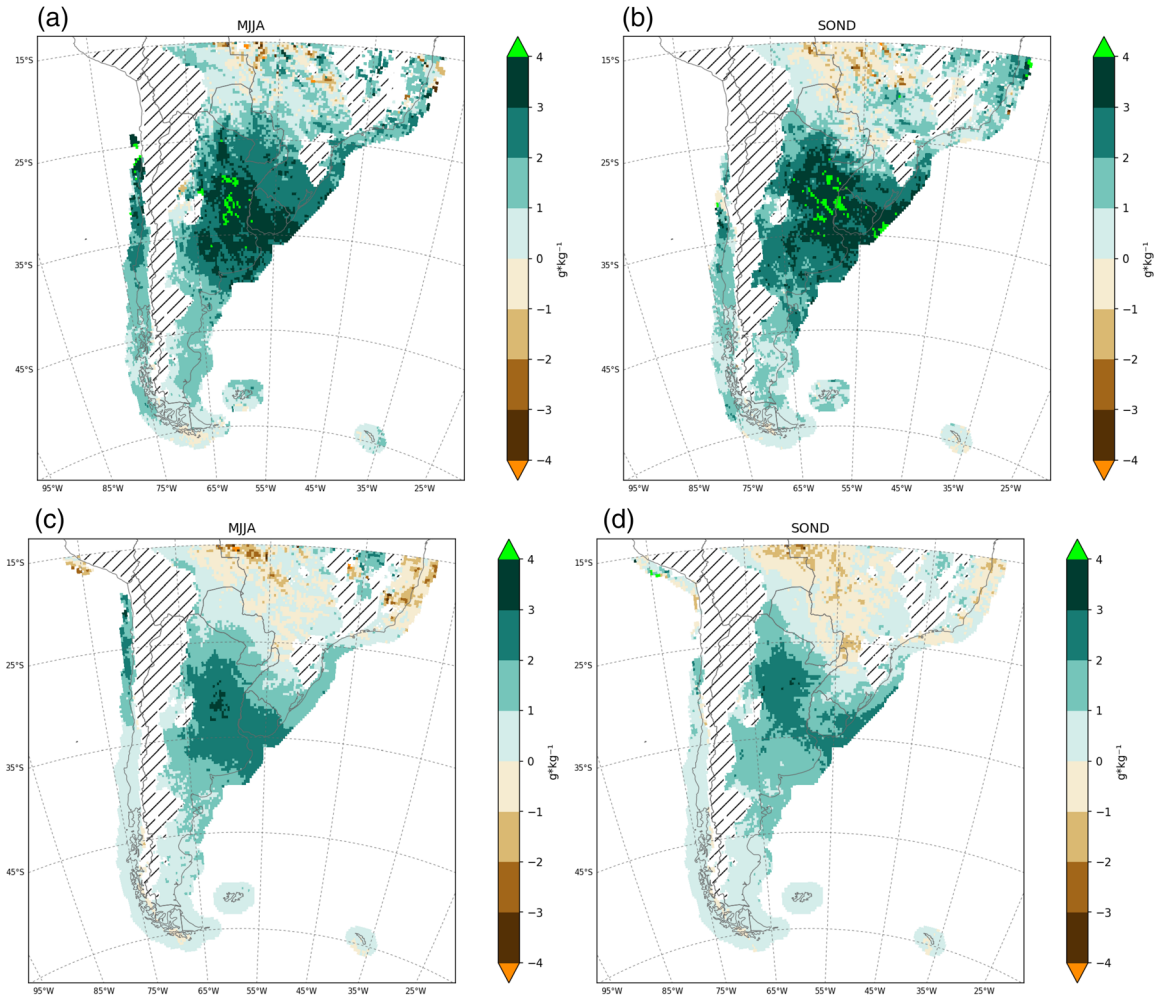

FIGURE 9 Top row: mean specific humidity anomaly for fronts that produce extreme precipitation for (a) MJJA, (b) SOND. Bottom row: mean specific humidity anomaly for fronts that produce precipitation for (c) MJJA, (d) SOND. Units are g·kg^{-1} [Colour figure can be viewed at wileyonlinelibrary.com]

availability at lower levels of the atmosphere is a key ingredient in feeding the system. Therefore, the specific humidity anomaly at the 850 hPa level is used as a measure of the available moisture for precipitating fronts. The anomaly is taken using the climatological monthly mean on each grid point. The choice of the climatological monthly mean instead of the climatological seasonal mean is because the specific humidity has a high variability. Also, since the specific humidity varies greatly with latitude, the anomaly is preferred as a way to easily identify the available moisture filtering the meridional changes.

Figure 9 displays the mean specific humidity anomaly for both types of precipitation-producing fronts in each season. In mid-latitudes, these mean anomalies are positive, with higher values located over central and northern Argentina. However, when comparing within the same region, the values associated with extreme-precipitation-producing fronts (Figure 9a,b) are higher (about $\sim$1 g·kg^{-1}) than those of the precipitating fronts (Figure 9c,d). These results could be equivalent to those described by Catto and Pfahl (2013), who found that, in mid-latitudes on both hemispheres, fronts that produce precipitation extremes have a much stronger wet bulb potential temperature gradient than other fronts. Furthermore, since in this study the temperature gradient appears not to be a distinguishing factor, the differences in the potential wet bulb temperature might be due to moisture differences, with higher values associated with extreme precipitation events.

To summarize, both the availability of moisture in lower levels and the stronger relative cyclonic vorticity are average distinctive characteristics of fronts that produce extreme precipitation. Hence, they could potentially aid in forecasting extreme precipitation events caused by fronts. Moreover, the dynamic forcing prevails over the thermodynamic forcing and this could mean steeper slopes in fronts associated with extreme precipitation.

4 | SUMMARY AND CONCLUSIONS

The relationship between fronts and extreme precipitation over southern South America was analysed in this study for two seasons: extended winter (from May to August) and extended spring (from September to December). This analysis was based on the 1979–2017 period. Daily gridded precipitation data was taken from the CPC Global Unified Precipitation while 850 hPa temperature, wind horizontal components, and specific humidity, as well as the terrain elevation, were taken from the ERA5 reanalysis.

To begin with, front intensity and frequency were characterized by means of the objective front index FI; FI combines cyclonic vorticity with thermal contrast—two fundamental characteristics of these mid-latitude systems—to identify fronts. This index was originally developed by Solman and Orlanski (2010) but two key filtering conditions were added in this study: first, a stricter terrain masking condition was applied, retaining only the regions where the 850 hPa level is mostly unaffected by the closeness to the surface level; secondly, a nonpersistent condition was used to keep transient perturbations and filter nonfrontal semipermanent features. Extreme precipitation was characterized in each season by means of the 95th percentile, taking into account both the threshold provided by this statistic and the number of days on which it was surpassed. Next, the percentage of total and extreme precipitation explained by fronts was calculated; the classification of precipitation as either frontal or nonfrontal was achieved by using an organic methodology that handles different latitudes equally. Lastly, several characteristics of precipitating fronts were compared with those of fronts that produce extreme precipitation in search of distinctive characteristics that could aid in frontal extreme precipitation forecasting.

Over southern South America, front frequency is about 10% and a seasonal shift is evidenced in the increased (decreased) frequency in southern (central and northern) Argentina in the extended spring when compared to the extended winter. The mean seasonal intensity—calculated as the seasonal mean of FI—is greater in winter (MJJA) than in spring (SOND); however, the spatial pattern is similar on both seasons. There are two relative minimums, one over the Eastern Pacific Ocean and the other over the Argentinean Sea. The weakest values are located north of 20°S where fronts are scarce while the highest values—associated with intense vorticity and thermal contrast—flank the Andes and some coastal areas.

The number of extreme precipitation days is less than 2.5% of the total number of days in each season for the study period. Regions with a higher (lower) number of extreme precipitation days also have higher (lower) 95th percentile values. The lowest 95th percentile values were found over the South American arid diagonal where the number of extreme precipitation days accounted for less than 1% of the total number of days. On the other hand, the highest values on mid-latitudes were found over SESA accounting for about 1.5% of the total number of days. Over this same region, there was an increase of both the number of extreme precipitation days and the 95th percentile values in spring compared to winter. A marked seasonal shift was found in northwestern Argentina where very low values in winter became substantially higher in spring.

Because fronts are mid-latitude systems, frontal precipitation over South America is mostly confined south of 20°S. In winter, frontal precipitation amounts to 50% of extreme precipitation, while in spring—as other forcing mechanisms become more relevant—fronts explain about 40% of the extreme precipitation. There is also a clear seasonal shift on the northern part of the region with frontal precipitation that is evidenced by a low percentage (less than 20%) of extreme precipitation explained by fronts in spring. While the spatial distribution of total precipitation explained by fronts is similar to the one of extreme precipitation explained by fronts, the percentage explained in the former case is lower (up to 40% in winter, and lower in spring). Consequently, fronts are an important forcing mechanism in triggering precipitation—especially, extreme events—in southern South America.

Fronts that produce extreme precipitation are, on average, more intense (i.e., have higher values of FI) than both precipitating fronts and all fronts but show essentially no seasonal differences between winter and spring. Furthermore, this stronger intensity is mostly attributed to the dynamic factor (cyclonic vorticity) while the thermodynamic factor (thermal contrast) is not effective in distinguishing fronts that produce extreme precipitation from the ones producing any kind of precipitation. Another key differentiating characteristic between these two types of fronts is the available moisture; while fronts that produce precipitation are associated with positive specific humidity anomalies, fronts producing extreme precipitation have, on average, higher anomalies at any given region. In conclusion, fronts that produce extreme precipitation have a stronger (dynamic) forcing coupled with a higher moisture availability. Hence, these two characteristics are the most promising to improve the forecasting of extreme precipitation caused by fronts.

ACKNOWLEDGEMENTS

The authors would like to thank the anonymous reviewers for their insightful comments that helped

improve the manuscript. This work has been supported by UBACYT2018 Grant 20020170100117BA, FONCYT Grant PICT2018-02496 and UNLP Grant PPID/G006. This work was carried out within the framework of an EVC-CIN 2019 scholarship.

AUTHOR CONTRIBUTIONS

Florencia I. Solari: Conceptualization; formal analysis; investigation; methodology; writing – original draft. **Josefina Blázquez:** Conceptualization; formal analysis; methodology; supervision; writing – review and editing. **Silvina A. Solman:** Conceptualization; formal analysis; methodology; supervision; writing – review and editing.

ORCID

Florencia I. Solari https://orcid.org/0000-0001-5281-9227
Josefina Blázquez https://orcid.org/0000-0003-3276-012X
Silvina A. Solman https://orcid.org/0000-0001-6693-9393

REFERENCES

Berry, G., Reeder, M.J. and Jakob, C. (2011) A global climatology of atmospheric fronts. *Geophysical Research Letters*, 38(4), L04809. https://doi.org/10.1029/2010GL046451.

Bjerknes, J. and Solberg, H. (1922) Life cycle of cyclones and the polar front theory of atmospheric circulation. By J. Bjerknes and H. Solberg. Kristiania, Geophysisks Publikationer, 3, 1922, No. 1. Pp. 18. 4°. Price 2 kr. *Quarterly Journal of the Royal Meteorological Society*, 49(206), 140–141.

Blázquez, J. and Solman, S.A. (2016) Intraseasonal variability of wintertime frontal activity and its relationship with precipitation anomalies in the vicinity of South America. *Climate Dynamics*, 46(7–8), 2327–2336. https://doi.org/10.1007/s00382-015-2704-0.

Blázquez, J. and Solman, S.A. (2017) Interannual variability of the frontal activity in the Southern Hemisphere: relationship with atmospheric circulation and precipitation over southern South America. *Climate Dynamics*, 48(7–8), 2569–2579. https://doi.org/10.1007/s00382-016-3223-3.

Blázquez, J. and Solman, S.A. (2018) Fronts and precipitation in CMIP5 models for the austral winter of the Southern Hemisphere. *Climate Dynamics*, 50(7–8), 2705–2717. https://doi.org/10.1007/s00382-017-3765-z.

Blázquez, J. and Solman, S.A. (2019) Relationship between projected changes in precipitation and fronts in the austral winter of the Southern Hemisphere from a suite of CMIP5 models. *Climate Dynamics*, 52(9–10), 5849–5860. https://doi.org/10.1007/s00382-018-4482-y.

Bluestein, H.B. (1993) *Synoptic-dynamic Meteorology in Midlatitudes. II. Observations and Theory of Weather Systems*. New York, NY: Oxford University Press.

Browning, K.A. and Roberts, N.M. (1994) Structure of a frontal cyclone. *Quarterly Journal of the Royal Meteorological Society*, 120(520), 1535–1557. https://doi.org/10.1002/qj.49712052006.

Bruniard, E.D. (1982) La diagonal árida Argentina: un límite climático real. *Revista Geografica*, 95, 5–20.

Carleton, T.A. and Hsiang, S.M. (2016) Social and economic impacts of climate. *Science*, 353(6304), aad9837. https://doi.org/10.1126/science.aad9837.

Catto, J.L., Jakob, C., Berry, G. and Nicholls, N. (2012) Relating global precipitation to atmospheric fronts. *Geophysical Research Letters*, 39(10), L10805. https://doi.org/10.1029/2012GL051736.

Catto, J.L. and Pfahl, S. (2013) The importance of fronts for extreme precipitation. *Journal of Geophysical Research: Atmospheres*, 118(19), 10–791. https://doi.org/10.1002/jgrd.50852.

Catto, J.L., et al. (2014) Atmospheric fronts in current and future climates. *Geophysical Research Letters*, 41(21), 7642–7650.

Cavalcanti, I.F.A. (2012) Large scale and synoptic features associated with extreme precipitation over South America: a review and case studies for the first decade of the 21st century. *Atmospheric Research*, 118, 27–40. https://doi.org/10.1016/j.atmosres.2012.06.012.

Dereczynski, C., et al. (2020) Downscaling of climate extremes over South America—part I: model evaluation in the reference climate. *Weather and Climate Extremes*, 29, 100273. https://doi.org/10.1016/j.wace.2020.100273.

Dowdy, A.J. and Catto, J.L. (2017) Extreme weather caused by concurrent cyclone, front and thunderstorm occurrences. *Scientific Reports*, 7, 40359. https://doi.org/10.1038/srep40359.

Escobar, G., et al. (2019) Climatology of surface baroclinic zones in the coast of Brazil. *Atmosfera*, 32, 129–141. https://doi.org/10.20937/atm.2019.32.02.04.

Garreaud, R.D., et al. (2009) Present-day south american climate. *Palaeogeography, Palaeoclimatology, Palaeoecology*, 281(3–4), 180–195. https://doi.org/10.1016/j.palaeo.2007.10.032.

Garreaud, R.D. (2000) Cold air incursions over subtropical South America: mean structure and dynamics. *Monthly Weather Review*, 128(7), 2544–2559.

Haylock, M.R., et al. (2006) Trends in total and extreme South American rainfall in 1960–2000 and links with sea surface temperature. *Journal of Climate*, 19(8), 1490–1512. https://doi.org/10.1175/JCLI3695.1.

Hersbach, H., Bill, B., Paul, B., Shoji, H., András, H., Joaquín, M.-S., Julien, N., Carole, P., Raluca, R., Dinand, S., Adrian, S., Cornel, S., Saleh, A., Xavier, A., Gianpaolo, B., Peter, B., Gionata, B., Jean, B., Massimo, B., Giovanna, C., Per, D., Dick, D., Michail, D., Rossana, D., Johannes, F., Richard, F., Manuel, F., Alan, G., Leo, H., Sean, H., Hogan, R. J., Elías, H., Marta, J., Sarah, K., Patrick, L., Philippe, L., Cristina, L., Gabor, R., Patricia, R., Iryna, R., Freja, V., Sebastien, V. and Jean-Noël, T. (2020) The ERA5 global reanalysis. *Quarterly Journal of the Royal Meteorological Society*, 146(730), 1999–2049. https://doi.org/10.1002/qj.3803.

Hewson, T.D. (1998) Objective fronts. *Meteorological Applications*, 5(1), 37–65.

Hirata, F.E. and Grimm, A.M. (2016) The role of synoptic and intraseasonal anomalies in the life cycle of summer rainfall extremes over South America. *Climate Dynamics*, 46(9–10), 3041–3055. https://doi.org/10.1007/s00382-015-2751-6.

Hirata, F.E. and Grimm, A.M. (2017) The role of synoptic and intraseasonal anomalies on the life cycle of rainfall extremes over South America: non-summer conditions. *Climate Dynamics*, 49(1–2), 313–326. https://doi.org/10.1007/s00382-016-3344-8.

Hope, P., Kevin, K., Michael, P., Jennifer, C., Ian, S., Graham, M., Peter, M., James, R. and Gareth, B. (2014) A comparison of automated methods of front recognition for climate studies: a case study in Southwest Western Australia. *Monthly Weather Review*, 142(1), 343–363. https://doi.org/10.1175/MWR-D-12-00252.1.

Lackmann, G. (2011) *Midlatitude Synoptic Meteorology*. Boston, MA: American Meteorological Society.

Loikith, p.C., Albertani, p.L., Emily, S., Judah, D., Mechoso, C.R. and Armineh, B. (2019) A climatology of daily synoptic circulation patterns and associated surface meteorology over southern South America. *Climate Dynamics*, 53(7), 4019–4035. https://doi.org/10.1007/s00382-019-04768-3.

Masson-Delmotte, V., et al. (2021) *IPCC 2021: Climate Change 2021: The Physical Science Basis. Contribution of Working Group I to the Sixth Assessment Report of the Intergovernmental Panel on Climate Change*. Cambridge: Cambridge University Press (in press).

Parfitt, R., Arnaud, C. and Hyodae, S. (2017) A simple diagnostic for the detection of atmospheric fronts. *Geophysical Research Letters*, 44(9), 4351–4358. https://doi.org/10.1002/2017GL073662.

Penalba, O.C. and Robledo, F.A. (2010) Spatial and temporal variability of the frequency of extreme daily rainfall regime in the La Plata Basin during the 20th century. *Climatic Change*, 98(3–4), 531–550. https://doi.org/10.1007/s10584-009-9744-6.

Re, M. and Barros, V.R. (2009) Extreme rainfalls in se South America. *Climatic Change*, 96(1–2), 119–136. https://doi.org/10.1007/s10584-009-9619-x.

Reboita, M.S., Alonso, G.M., da Porfírio, R.R. and Tércio, A. (2010) Regimes de precipitação na América do Sul: uma revis∼ao bibliográfica. *Revista Brasileira de Meteorologia*, 25, 185–204. https://doi.org/10.1590/S0102-77862010000200004.

Reboita, M.S., et al. (2022) South America climate change revealed through climate indices projected by GCMs and Eta-RCM ensembles. *Climate Dynamics*, 58(1), 459–485. https://doi.org/10.1007/s00382-021-05918-2.

Rudeva, I., Ian, S., David, C. and Ghyslaine, B. (2019) Midlatitude fronts and variability in the Southern Hemisphere tropical width. *Journal of Climate*, 32(23), 8243–8260. https://doi.org/10.1175/JCLI-D-18-0782.1.

Satyamurty, P., et al. (1998) South America. In: *Meteorology of the Southern Hemisphere*. Boston, MA: Springer, pp. 119–139.

Schemm, S., Irina, R. and Ian, S. (2015) Extratropical fronts in the lower troposphere–global perspectives obtained from two automated methods. *Quarterly Journal of the Royal Meteorological Society*, 141(690), 1686–1698. https://doi.org/10.1002/qj.2471.

Simmonds, I., Kevin, K. and Arthur, T.B.J. (2012) Identification and climatology of Southern Hemisphere mobile fronts in a modern reanalysis. *Journal of Climate*, 25(6), 1945–1962. https://doi.org/10.1175/JCLI-D-11-00100.1.

Sinnott, R.W. (1984) Virtues of the Haversine. *S&T*, 68(2), 158.

Solman, S.A. and Orlanski, I. (2010) Subpolar high anomaly preconditioning precipitation over South America. *Journal of the Atmospheric Sciences*, 67(5), 1526–1542. https://doi.org/10.1175/2009JAS3309.1.

Solman, S.A. and Orlanski, I. (2014) Poleward shift and change of frontal activity in the Southern Hemisphere over the last 40 years. *Journal of the Atmospheric Sciences*, 71(2), 539–552. https://doi.org/10.1175/JAS-D-13-0105.1.

Urraca, R., Thomas, H., Ana, G.-A., Francisco Javier, M.P., Frank, K. and Andres, S.-G. (2018) Evaluation of global horizontal irradiance estimates from ERA5 and COSMO-REA6 reanalyses using ground and satellite-based data. *Solar Energy*, 164, 339–354. https://doi.org/10.1016/j.solener.2018.02.059.

Vörösmarty, C.J., et al. (2013) Extreme rainfall, vulnerability and risk: a continental-scale assessment for South America. *Philosophical Transactions of the Royal Society A: Mathematical, Physical and Engineering Sciences*, 371(2002), 20120408. https://doi.org/10.1098/rsta.2012.0408.

Wu, Y. and Polvani, L.M. (2017) Recent trends in extreme precipitation and temperature over southeastern South America: the dominant role of stratospheric ozone depletion in the CESM large ensemble. *Journal of Climate*, 30(16), 6433–6441. https://doi.org/10.1175/JCLI-D-17-0124.1.

Xie, P., et al. (2010) CPC unified gauge-based analysis of global daily precipitation. In: *24th Conference on Hydrology, Atlanta, GA*, Vol. 2. Boston, MA: American Meteorological Society.

How to cite this article: Solari, F. I., Blázquez, J., & Solman, S. A. (2022). Relationship between frontal systems and extreme precipitation over southern South America. *International Journal of Climatology*, 1–15. https://doi.org/10.1002/joc.7663